Improved Beamforming in 3D Space Applied to Realistic Planar Antenna Arrays by Using the Embedded Element Patterns

Zaharias D. Zaharis, *Senior Member, IEEE,* Ioannis P. Gravas, Pavlos I. Lazaridis, *Senior Member, IEEE,* Traianos V. Yioultsis, *Member, IEEE,* and Thomas D. Xenos

***Abstract*—Most of beamforming methods rely on the proper estimation of the steering vectors of the incoming signals in order to calculate appropriate array feeding weights. However, this estimation is often performed on a theoretical basis, since most methods assume that the array elements radiate like isotropic sources and consider only the phase differences between them due to their different spatial positions. This is a rough estimation as it ignores both the non-isotropic radiation pattern of the array elements and the mutual coupling between them. To overcome these limitations, we use a different approach for the construction of steering vectors based on the embedded patterns of the array elements, extracted through full-wave analysis. This approach is used in this paper to modify two well-known beamforming methods, namely the null steering beamforming and the minimum variance distortionless response method. Both modified methods are applied to a realistic model of a microstrip planar antenna array, and thus, both the azimuth and polar angles of the main lobe and nulls directions are controlled (beamforming in 3D space). Extensive statistical analyses are performed by implementing several scenarios of escalating difficulty, in order to examine the performance and temporal response of the modified beamforming methods in comparison to the respective conventional methods and also in comparison to beamforming methods based on evolutionary techniques.**

***Index Terms*—Beamforming, embedded element pattern, minimum variance distortionless response (MVDR), null steering beamforming (NSB), planar antenna arrays.**

Manuscript received February 28, 2022. This research was supported by Greece and the European Union (European Social Fund-ESF) through the Operational Programme "Human Resources Development, Education and Lifelong Learning" in the context of the project "Strengthening Human Resources Research Potential via Doctorate Research" (MIS-5000432), implemented by the State Scholarships Foundation (IKY). Also, this research was supported by the European Union, partially through the Horizon 2020 Marie Skłodowska-Curie Innovative Training Networks Programme "Mobility and Training for beyond 5G Ecosystems (MOTOR5G)" under grant agreement no. 861219, and partially through the Horizon 2020 Marie Skłodowska-Curie Research and Innovation Staff Exchange Programme "Research Collaboration and Mobility for Beyond 5G Future Wireless Networks (RECOMBINE)" under grant agreement no. 872857. (*Corresponding author: Zaharias D. Zaharis*)

Z. D. Zaharis, I. P. Gravas, T. V. Yioultsis, and T. D. Xenos are with the School of Electrical and Computer Engineering, Aristotle University of Thessaloniki, 54124 Thessaloniki, Greece (e-mail: zaharis@auth.gr; igravas@auth.gr; traianos@auth.gr; tdxenos@auth.gr).

P. I. Lazaridis is with the Department of Engineering and Technology, University of Huddersfield, Huddersfield HD1 3DH, U.K. (e-mail: p.lazaridis@hud.ac.uk).

I. Introduction

ADAPTIVE beamforming (ABF) refers to a real time procedure that calculates the appropriate complex feeding weights (amplitudes and phases) of an antenna array in order to concurrently steer the main lobe towards the direction of arrival (DOA) of a desired incoming signal (DIS), and place nulls towards DOAs of undesired incoming signals (UISs), as shown in Fig. 1 [1]–[15]. The ABF process performed when the antenna array operates in reception mode is quite different from the ABF process in transmission mode. In reception mode, the process is much simpler, because the feeding weights are calculated and implemented through algorithmic procedures. Practically, in reception mode, only signal processing takes place, in order to remove the effect of UISs at the beamformer output. On the contrary, when the antenna array operates in transmission mode, the ABF process becomes more complex. In this case, the feeding weights must be implemented in a hardware-based manner (i.e., represented by currents with certain amplitudes and phases) by using complex active electronic circuits.

So far, beamforming methods have been used in many applications in practice [16]–[26]. In general, three main types of ABF algorithms can be found in the literature depending on how the feeding weights are calculated:

1) Deterministic ABF algorithms [1]–[9], which provide an instant calculation of the feeding weights,
2) iterative ABF algorithms [10]–[15], [27], that provide an optimal solution after a number of iterations, and
3) neural network (NN) based ABF algorithms [28]–[31], which also provide an instant response, but need extensive training before they can be employed, and are applicable only in the area where the training data were collected.

So far, iterative ABF algorithms have been based on either optimization algorithms [10], [12]–[14] or successive fast Fourier transformations [11], [15]. In real-world applications, DOA of DIS or DOA of a UIS may change in real time, and thus the feeding weights need to be recalculated, when such a change occurs. Therefore, iterative ABF algorithms are not an efficient choice, if a large number of iterations is required to obtain an optimal solution, because in such cases the beamformer needs a considerable amount of time to respond properly. This will become evident by the statistical analysis shown in section IX. Thus, much faster computational

hardware (CPUs or GPUs) must be employed to compensate somewhat for the delayed response of such beamformers. On the other hand, NN-based beamformers are able to provide instant response due to the nature of NNs, but need a lot of data and time in order to be effectively trained, and therefore their good performance can be ensured only in stable or slowly-changing electromagnetic (EM) environments. Unlike iterative ABF algorithms, a deterministic ABF algorithm is capable of providing immediate response because it has either non-iterative structure or a structure with a small number of iterations. In addition, unlike NN-based beamformers, a deterministic ABF algorithm is capable of providing accurate response in ever-changing environments without the need for prior training. From all the above, it is evident that deterministic ABF algorithms are the most suitable candidates for ever-changing environments.

To calculate the appropriate feeding weights, many ABF methods rely on the estimation of the steering vectors of the incoming signals. Most of them construct the steering vectors by treating the array elements as isotropic sources, thus ignoring the non-isotropic radiation pattern of each element and the mutual coupling between them. As a result, they assume that the radiation pattern is only expressed by the array factor (AF). Under this consideration, the steering vectors are constructed by simply taking into account the phase differences between the electric fields of the array elements (treated as point sources) due to their relative spatial positions. Many methods [32]–[39] have been proposed to estimate and incorporate the effects of mutual coupling in antenna arrays. Among them, some perform the calculation of the mutual coupling coefficients and construct the corresponding mutual coupling matrix (MCM) [34]–[37], [39], while other methods use orthogonal expressions [33] or virtual active element pattern expansions [38]. Such methods rely on complex calculations and estimations, which may slow down the weight calculation process. There are also studies that focus on a hardware-based reduction of mutual coupling by proposing new antenna designs [40] that mitigate this coupling.

In this paper, a different approach is employed to construct the steering vectors [41]. In particular, these vectors are built by using the embedded patterns of the array elements [42], [43]. The so-called "embedded element pattern" (EEP) refers to the radiation pattern of an M-element antenna array, when only one element is driven by a source and all the other elements $(M-1)$ are non-driven. By driving a different element each time and keeping the rest of the elements non-driven, a separate EEP is produced. In this way, M separate EEPs can be produced in total.

Depending on the type of the source considered for driving the elements, a different type of EEP can be produced:

1) If an ideal current source is considered (meaning that the source has no internal impedance connected in parallel), then the non-driven elements will have their feeding terminals open-circuited, and therefore a set of M open-circuited EEPs (OCEEPs) will be produced [43].
2) If an ideal voltage source is considered (meaning that the source has no internal impedance connected in series), then the non-driven elements will have their feeding terminals short-circuited, and therefore a set of M short-circuited EEPs (SCEEPs) will be produced.
3) If a practical (non-ideal) current source is considered (meaning that there is an internal impedance connected to the source in parallel), then the non-driven elements will have their feeding terminals connected to loads equal to the internal source impedance. In this way, a set of M loaded EEPs (LEEPs) will be produced.
4) If a practical (non-ideal) voltage source is considered (meaning that there is an internal impedance connected to the source in series), then the non-driven elements will have their feeding terminals connected to loads equal to the internal source impedance. In this way, a set of M loaded EEPs (LEEPs) will be produced again.

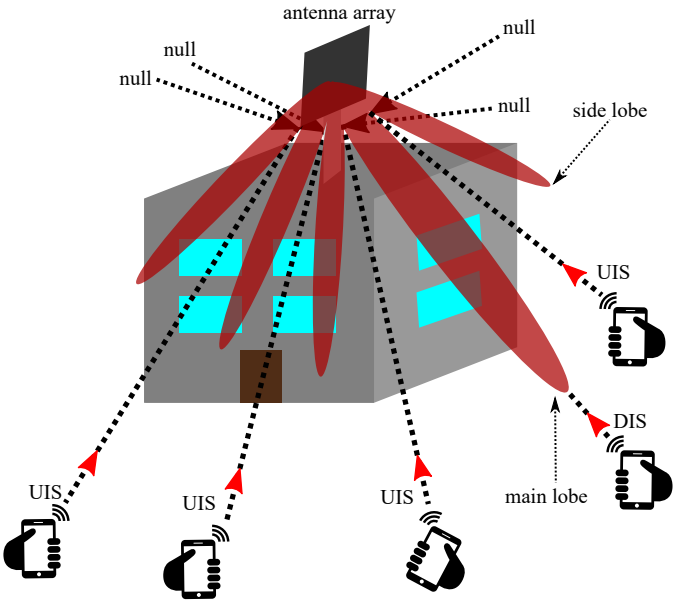

Fig. 1. A base station antenna in reception mode, serving a single user (DIS) at a given time, while reducing interference from several UISs at the same time by placing radiation pattern nulls towards their DOAs.

In this paper, the CST software package [44] has been employed to perform full-wave analysis of the antenna array, and thus to produce the set of M EEPs. These EEPs are actually LEEPs, due to the use of practical (non-ideal) current sources in the CST environment. The internal source impedance considered in the CST calculations is equal to the usual reference impedance of 50 Ω. It has to be pointed out that EEPs have already been used in beamformers based on evolutionary algorithms such as the particle swarm optimization (PSO) [45], [46]. However, as previously explained, beamformers based on evolutionary algorithms are not so suitable for real-time applications, because they need a considerable amount of time to provide an optimal solution, as shown in section IX.

In order to produce LEEPs using CST, we extract M distributions in 3D space of M respective electric field components (E_ϕ or E_θ) through full-wave analysis, all produced by the whole antenna array, but for each distribution only one of the M elements is driven with a unitary weight (i.e., $1+j0$) by a practical (non-ideal) current source, while all the other

elements are non-driven (connected to 50 Ω loads). For an M-element array, this process can be comprehended as a decomposition of the total electric field component (i.e., the electric field component E_ϕ or E_θ produced by the array when all its elements are driven) to M LEEPs, each one corresponding to the excitation of a specific array element. LEEPs have complex values as they represent electric field components. Once the values of LEEPs are defined for every pair of angles of interest (θ, ϕ), in a spherical sector, according to a desired stepsize, they are permanently saved into matrices, and then every steering vector can be instantly constructed from the complex values of LEEPs at DOA (θ, ϕ) of the respective incoming signal.

With this approach, it is expected that the feeding weights will lead to a more precise main lobe and nulls placement, because both the non-isotropic radiation pattern of the array elements and the mutual coupling between them are now taken into account. The distribution in 3D space of the total electric field component E_ϕ or E_θ produced by the whole array, when all of its elements are driven using a set of feeding weights, can be easily calculated as a linear combination of LEEPs using these weights. Consequently, the radiation pattern calculated in this way is much closer to reality as both the mutual coupling and the actual radiation pattern of each array element are taken into account. Based on all the above, it is expected that, by using this approach for steering vector construction, much more accurate feeding weights will be calculated and more precise main lobe and nulls placement will be achieved. It must also be clarified that this approach can be applied to any antenna array type or geometry, as long as LEEPs of the array in use are available.

For the purpose of this study, we use the above-mentioned methodology to modify two well-known ABF methods, namely the null steering beamforming (NSB) and the minimum variance distortionless response (MVDR) methods, which will be used to achieve high precision beamforming. A 64-element (8×8) microstrip planar antenna array (MPAA) has been modeled and simulated in the CST environment in order to derive, through full-wave analysis, 64 LEEPs. The antenna array is designed for operation at 800 MHz, i.e., for operation in the n20 band of 5G wireless communications. In practice, the antenna array is usually located at a certain height above the ground (see Fig. 2). Due to its position and its planar geometry, the array may receive incoming signals only within a certain spherical sector, which is defined here by values of the polar angle θ within the angular sector $[90°, 150°]$ and values of the azimuth angle ϕ within $[-45°, 45°]$.

The validity of the new approach is tested by simulating the antenna array in the CST environment using feeding weights calculated by the modified ABF methods, and by verifying that the radiation pattern produced by this simulation is in good agreement with the radiation pattern produced by the linear combination of LEEPs using these weights. Also, extensive statistical analyses have been performed for both modified methods in order to prove the effectiveness of the new approach in terms of the divergences of the main lobe and nulls directions from their respective expected directions, and the signal to interference-plus-noise ratio (SINR). The new

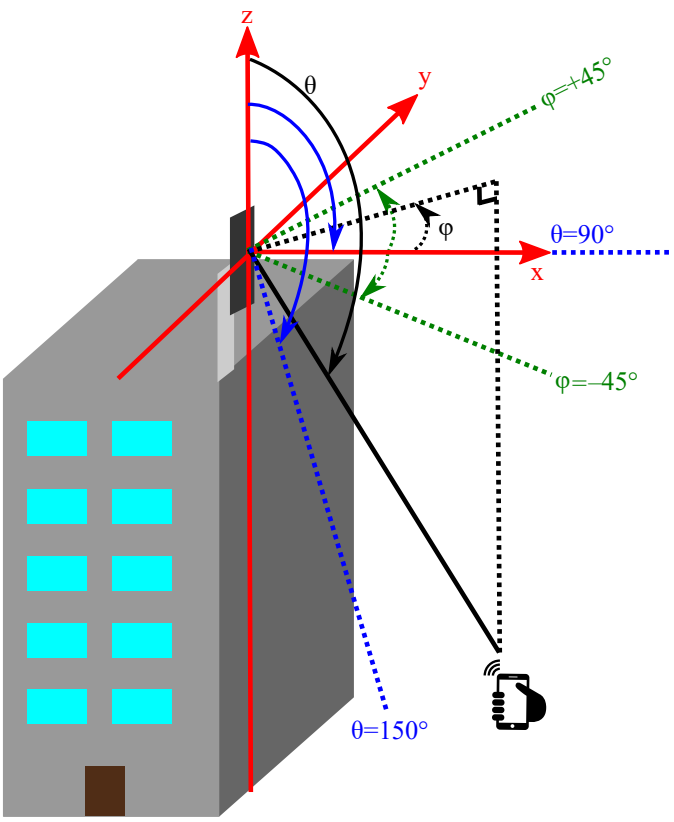

Fig. 2. Realistic beamforming system incorporating a planar antenna array located at a certain height above the ground and serving any user equipment within a certain spherical sector.

approach shows excellent accuracy in the placement of nulls with near-zero divergences, minor main lobe divergences and excellent SINR values in all test scenarios.

The contribution of this paper is the replacement of the theoretical steering vectors, used in conventional beamforming methods, with LEEP-based steering vectors. These new steering vectors are realistic, because they incorporate information about the antenna array in use, such as the mutual coupling between the array elements and the individual radiation pattern of each array element. Therefore, the use of LEEP-based steering vectors improves the accuracy of the beamforming methods, because the realistic behavior of the antenna array in use is taken into account. Also, since the LEEP-based steering vectors depend on the type or geometry of the antenna array, it is evident that the modified beamforming methods can be applied to any type or geometry of antenna array, as long as LEEPs of the array in use are available. Moreover, the modified beamforming methods provide the same immediate response as the conventional methods, because once the M LEEPs have been calculated by full-wave analysis, their values can be saved for permanent use in the beamformer storage, and then the feeding weights can instantly be calculated by the modified methods by constructing the steering vectors of any incoming signals from LEEPs. Finally, we gain both in computational speed and storage, since only one electric field component is used, as shown in section III.

II. Conventional Beamforming Approach

According to the conventional ABF problem, N signals s_n $(n = 1, 2, \ldots, N)$ are received by an M-element antenna array (with $M > N$) at frequency f (wavelength λ). From them, s_1 is DIS and the rest $N-1$ are UISs. The DOA of the nth signal $(n = 1, 2, \ldots, N)$ is defined by a pair of angles (θ_n, ϕ_n). Most beamforming methods in literature are based on a simplified model that treats the array elements as isotropic sources and ignores the mutual coupling between them. Thus, they consider that the radiation pattern of the antenna array is expressed by the array factor:

$$\mathrm{AF}(\theta, \phi) = \sum_{m=1}^{M} w_m^* \exp\left(j\beta \vec{r}_m \cdot \vec{v}(\theta, \phi)\right), \tag{1}$$

where w_m $(m = 1, 2, \ldots, M)$ is the feeding weight of the mth array element (actually, it represents the conjugate complex value of the respective excitation current at the input port of this element), β is the propagation phase constant $(\beta = 2\pi/\lambda)$, $\vec{r}_m$ is the position vector of the mth array element (its expression depends on the array geometry),

$$\vec{v}(\theta, \phi) = \cos\phi \sin\theta \ \vec{x}_0 + \sin\phi \sin\theta \ \vec{y}_0 + \cos\theta \ \vec{z}_0 \tag{2}$$

is the direction unit vector, and finally $\vec{x}_0, \vec{y}_0$ and $\vec{z}_0$ are the respective unit vectors of x, y and z-axes. According to most ABF methods, the theoretical steering vector that corresponds to an incoming signal received by an M-element array at DOA (θ, ϕ) is given by:

$$\mathbf{a}(\theta, \phi) = \begin{bmatrix} \exp\left(j\beta \vec{r}_1 \cdot \vec{v}(\theta, \phi)\right) \\ \exp\left(j\beta \vec{r}_2 \cdot \vec{v}(\theta, \phi)\right) \\ \vdots \\ \exp\left(j\beta \vec{r}_M \cdot \vec{v}(\theta, \phi)\right) \end{bmatrix}. \tag{3}$$

By taking into account (3), we can rewrite (1) in terms of matrix notation as:

$$\mathrm{AF}(\theta, \phi) = \mathbf{w}^{\mathrm{H}} \mathbf{a}(\theta, \phi), \tag{4}$$

where

$$\mathbf{w} = \begin{bmatrix} w_1 & w_2 & \cdots & w_M \end{bmatrix}^{\mathrm{T}} \tag{5}$$

is the excitation weight vector, while superscripts T and H denote the transpose operation and the Hermitian transpose operation, respectively.

It is evident from (3) that the theoretical steering vector treats the array elements as isotropic sources, and therefore it ignores the non-isotropic radiation pattern produced by these elements as well as the mutual coupling between them. Actually, the theoretical steering vector contains only information about the phase differences developed by an incoming signal at the inputs of the M isotropic sources due to the different spatial positions of these sources. Many beamforming methods, such as [34]–[37], have been proposed so far for the estimation of the mutual coupling coefficients and the construction of the MCM, but they still ignore the non-isotropic pattern of the array elements. At the same time, the estimation of coupling coefficients requires complex calculations that slow down the beamformer response.

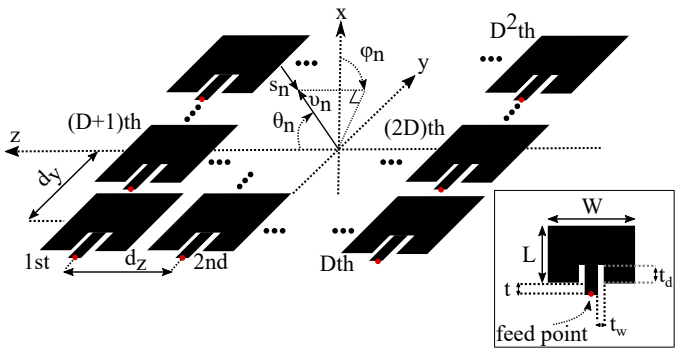

Fig. 3. Realistic M-element planar antenna array employed for beamforming.

III. Realistic Antenna Array Beamforming

Let us consider the general case of a $D \times D$ MPAA composed of rectangular microstrip elements placed parallel to the yz-plane, with element spacings d_y along the y-axis and d_z along the z-axis, as shown in Fig. 3. Due to the position of the feeding ports (see Fig. 3), there is a spherical sector where the theta-component E_θ of the total electric field produced by the MPAA is significantly smaller in amplitude compared to the phi-component E_ϕ (axial ratio greater than 20 dB) [47], [48]. Therefore, the total electric field of this array can be expressed only by E_ϕ. Thus, E_ϕ can be written as:

$$E_\phi(\theta, \phi) = \sum_{m=1}^{M} w_m^* e_{\phi m}(\theta, \phi), \tag{6}$$

where $M = D^2$ and $e_{\phi m}(\theta, \phi)$ $(m = 1, 2, \ldots, M)$ is the electric phi-component produced by the MPAA, when only the mth array element is driven with a unitary feeding weight by a practical current source, while all the other elements are non-driven. Practically, (6) shows that E_ϕ can be expressed as a superposition of M phi-components of LEEPs $e_{\phi m}$. To obtain realistic values of $e_{\phi m}(\theta, \phi)$, a full-wave analysis must be performed on the MPAA, and this can be achieved by employing any full-wave analysis software package. As a realistic term, $e_{\phi m}$ incorporates information related to the non-isotropic radiation pattern of the array elements and the mutual coupling between them. As previously mentioned, CST has been selected as EM-solver. By using matrix notation, (6) can be written as:

$$E_\phi(\theta, \phi) = \mathbf{w}^{\mathrm{H}} \mathbf{e}_\phi(\theta, \phi), \tag{7}$$

where

$$\mathbf{e}_\phi(\theta, \phi) = \begin{bmatrix} e_{\phi 1}(\theta, \phi) & e_{\phi 2}(\theta, \phi) & \cdots & e_{\phi M}(\theta, \phi) \end{bmatrix}^{\mathrm{T}} \tag{8}$$

is a vector composed of all electric phi-components $e_{\phi m}$ that correspond to DOA (θ, ϕ), and therefore is called the "electric phi-vector".

Equations (4) and (7) represent, respectively, the theoretical and the realistic radiation pattern produced by the whole array, and due to their resemblance in formulation, we realize that $\mathbf{e}_\phi(\theta, \phi)$ represents the realistic steering vector (LEEP-based steering vector). Consequently, if we replace $\mathbf{a}(\theta, \phi)$ with $\mathbf{e}_\phi(\theta, \phi)$ in any equation that applies to a theoretical antenna array, then the modified equation will apply to the realistic case

of this array. The replacement of $\mathbf{a}(\theta,\phi)$ with $\mathbf{e}_\phi(\theta,\phi)$ can be performed for any realistic antenna array type or geometry, as long as LEEPs of the array in use are available.

We denote as $x_m(k)$ $(m=1,2,\ldots,M)$ the signal induced at the input of the mth array element due to N incoming signals $s_n(k)$ plus a zero-mean additive Gaussian noise signal $n_m(k)$ $(m=1,2,...,M)$, with k indicating the kth time sample. The realistic values of x_m can be extracted by the expression

$$x_m(k)=\sum_{n=1}^{N} s_n(k)e_{\phi m}(\theta_n,\phi_n)+n_m(k), \tag{9}$$

which is a modification of the respective theoretical well-known expression, where all components of $\mathbf{a}(\theta,\phi)$ have been replaced with the respective components of $\mathbf{e}_\phi(\theta,\phi)$. Then, the total input vector, defined as

$$\mathbf{x}(k)=\begin{bmatrix}x_1(k) & x_2(k) & \cdots & x_M(k)\end{bmatrix}^{\mathrm{T}}, \tag{10}$$

can be estimated by the expression:

$$\mathbf{x}(k)=\mathbf{E}_\phi\mathbf{s}(k)+\mathbf{n}(k), \tag{11}$$

where

$$\mathbf{E}_\phi=\begin{bmatrix}\mathbf{e}_\phi(\theta_1,\phi_1) & \mathbf{e}_\phi(\theta_2,\phi_2) & \cdots & \mathbf{e}_\phi(\theta_N,\phi_N)\end{bmatrix} \tag{12}$$

is an $M\times N$ matrix, which represents the total realistic steering matrix according to our proposed approach, and therefore is called the "total electric phi-matrix",

$$\mathbf{s}(k)=\begin{bmatrix}s_1(k) & s_2(k) & \cdots & s_N(k)\end{bmatrix}^{\mathrm{T}} \tag{13}$$

is the incoming signal vector, and

$$\mathbf{n}(k)=\begin{bmatrix}n_1(k) & n_2(k) & \cdots & n_M(k)\end{bmatrix}^{\mathrm{T}} \tag{14}$$

is the noise vector. The output of the beamformer is given as:

$$y(k)=\mathbf{w}^{\mathrm{H}}\mathbf{x}(k). \tag{15}$$

Since realistic signal samples were not available in this study, the following reasonable assumptions were made to estimate the correlation matrices:

1) There is no correlation between any two incoming signals, and therefore the correlation matrix of the incoming signals $\mathbf{R}_{ss}$ can be approximated by a diagonal matrix. Furthermore, by assuming that all incoming signals have mean power equal to unity, i.e., $\hat{P}_{sn}=\mathrm{E}[s_n(k)s_n^*(k)]=1$, $n=1,\ldots,N$, ($\mathrm{E}[\cdot]$ denotes the expected value), $\mathbf{R}_{ss}$ can be further simplified into an $N\times N$ identity matrix, i.e., $\mathbf{R}_{ss}=\mathrm{E}[\mathbf{s}(k)\mathbf{s}^{\mathrm{H}}(k)]=\mathbf{I}_N$.
2) There is no correlation between any two noise signals, and therefore the noise correlation matrix $\mathbf{R}_{nn}$ ($M\times M$ matrix) can be approximated as:
$$\mathbf{R}_{nn}=\hat{P}_n\mathbf{I}_M, \tag{16}$$
where $\hat{P}_n=10^{-\mathrm{SNR}/10}$ is the mean noise power, $\mathbf{I}_M$ is the $M\times M$ identity matrix, and SNR is the signal to noise ratio in dB.
3) Finally, the incoming signals have no correlation with the noise signals.

By taking into account all the aforementioned assumptions, the input correlation matrix of the beamformer is defined as:

$$\begin{aligned}\mathbf{R}_{xx}&=\mathrm{E}[\mathbf{x}(k)\mathbf{x}^{\mathrm{H}}(k)]\\&=\mathbf{E}_\phi\,\mathrm{E}[\mathbf{s}(k)\mathbf{s}^{\mathrm{H}}(k)]\mathbf{E}_\phi^{\mathrm{H}}+\mathrm{E}[\mathbf{n}(k)\mathbf{n}^{\mathrm{H}}(k)]\\&=\mathbf{E}_\phi\mathbf{E}_\phi^{\mathrm{H}}+\mathbf{R}_{nn}\ .\end{aligned} \tag{17}$$

Due to the first of the above three assumptions, the correlation matrix of the interfering incoming signals is defined as:

$$\mathbf{R}_{ii}=\mathrm{E}[\mathbf{s}_i(k)\mathbf{s}_i^{\mathrm{H}}(k)]=\mathbf{I}_{N-1}, \tag{18}$$

where

$$\mathbf{s}_i(k)=\begin{bmatrix}s_2(k) & s_3(k) & \cdots & s_N(k)\end{bmatrix}^{\mathrm{T}} \tag{19}$$

is a column vector containing the kth samples of the interfering signals and $\mathbf{I}_{N-1}$ is the $(N-1)\times(N-1)$ identity matrix. By using (11), (12), and (19), (15) can further be analyzed as follows:

$$\begin{aligned}y(k)=&y_d(k)+y_u(k)=\mathbf{w}^{\mathrm{H}}\mathbf{e}_\phi(\theta_1,\phi_1)s_1(k)\\&+\mathbf{w}^{\mathrm{H}}\big[\mathbf{E}_{\phi i}\mathbf{s}_i(k)+\mathbf{n}(k)\big],\end{aligned} \tag{20}$$

where $y_d(k)$ is the desired component of the beamformer output that corresponds to DIS s_1, $y_u(k)$ is the undesired component that corresponds to all UISs plus noise, and $\mathbf{E}_{\phi i}$ is an $M\times(N-1)$ matrix similar to $\mathbf{E}_\phi$ in structure but composed only of the electric phi-vectors that correspond to UISs. The mean power of $y_d(k)$ is given as:

$$\begin{aligned}\hat{P}_{yd}=&\,\mathrm{E}\left[y_d(k)y_d^*(k)\right]\\=&\mathbf{w}^{\mathrm{H}}\mathbf{e}_\phi(\theta_1,\phi_1)\mathbf{e}_\phi^{\mathrm{H}}(\theta_1,\phi_1)\mathbf{w}.\end{aligned} \tag{21}$$

On the other hand, the mean power of $y_u(k)$ is given as:

$$\begin{aligned}\hat{P}_{yu}&=\mathrm{E}[y_u(k)y_u^*(k)]\\&=\mathbf{w}^{\mathrm{H}}\mathbf{E}_{\phi i}\mathbf{R}_{ii}\mathbf{E}_{\phi i}^{\mathrm{H}}\mathbf{w}+\mathbf{w}^{\mathrm{H}}\mathbf{R}_{nn}\mathbf{w}\\&=\mathbf{w}^{\mathrm{H}}\mathbf{E}_{\phi i}\mathbf{E}_{\phi i}^{\mathrm{H}}\mathbf{w}+\mathbf{w}^{\mathrm{H}}\mathbf{R}_{nn}\mathbf{w}.\end{aligned} \tag{22}$$

Finally, by dividing (21) by (22), we obtain the value of SINR in dB:

$$\mathrm{SINR}=10\log\frac{\hat{P}_{yd}}{\hat{P}_{yu}}. \tag{23}$$

IV. Modified Null Steering Beamforming

NSB [1] is a beamforming method, whose purpose is to keep DIS undistorted and eliminate all UISs received at known DOAs by the antenna array. To achieve this, the algorithm creates radiation pattern nulls at DOAs of UISs, thus maximizing the signal to interference ratio (SIR), and for that reason the NSB is also known in the literature as the maximum SIR beamformer. The weight calculation for $M>N$ according to the conventional NSB method is performed by using the expression:

$$\mathbf{w}_{\mathrm{NSB}}=\mathbf{A}(\mathbf{A}^{\mathrm{H}}\mathbf{A})^{-1}\mathbf{e}_1, \tag{24}$$

where

$$\mathbf{A}=\begin{bmatrix}\mathbf{a}(\theta_1,\phi_1) & \mathbf{a}(\theta_2,\phi_2) & \cdots & \mathbf{a}(\theta_N,\phi_N)\end{bmatrix} \tag{25}$$

is the total theoretical steering matrix, and

$$\mathbf{e}_1=\begin{bmatrix}1 & 0 & \cdots & 0\end{bmatrix}^{\mathrm{T}} \tag{26}$$

is a unit vector of size $N \times 1$. As explained in section III, by replacing the theoretical steering vector of every incoming signal with the respective realistic steering vector in any equation that applies to a theoretical antenna array, then the modified equation will apply to the realistic case of this array. In this way, $\mathbf{A}$ is replaced with $\mathbf{E}_\phi$, and therefore (24) is modified as follows:

$$\mathbf{w}_{\mathrm{NSB}} = \mathbf{E}_\phi(\mathbf{E}_\phi^{\mathrm{H}}\mathbf{E}_\phi)^{-1}\mathbf{e}_1, \tag{27}$$

The last expression is the modified NSB formula.

V. Modified Minimum Variance Distortionless Response

Contrary to NSB, which maximizes SIR, MVDR [1] is a beamforming method that aims to find the optimum feeding weights, which keep DIS undistorted at the output of the beamformer and minimize $\hat{P}_{yu}$ (interference-plus-noise mean power at the beamformer output), thus maximizing SINR. The MVDR solution is identical to the maximum likelihood solution, while providing the advantage that it does not require UISs and noise signals to follow a circularly-symmetric complex normal distribution, as demanded by the maximum likelihood method [2]. This advantage makes the MVDR solution more general. The weight calculation according to the conventional MVDR method is performed by using the expression:

$$\mathbf{w}_{\mathrm{MV}} = \mathbf{R}_{xx}^{-1}\mathbf{a}(\theta_1, \phi_1) \tag{28}$$

By replacing $\mathbf{a}(\theta_1, \phi_1)$ with $\mathbf{e}_\phi(\theta_1, \phi_1)$ and using (17), we extract the modified MVDR expression as follows:

$$\mathbf{w}_{\mathrm{MV}} = (\mathbf{E}_\phi\mathbf{E}_\phi^{\mathrm{H}} + \mathbf{R}_{nn})^{-1}\mathbf{e}_\phi(\theta_1, \phi_1) \tag{29}$$

VI. Optimization of Microstrip Planar Antenna Array

In this study, a 64-element ($D = 8$, $M = 64$) MPAA has been designed for operation at $f = 800$ MHz (n20 band of 5G wireless communications) and simulated in CST. The microstrip elements are considered to be rectangular and constructed according to the inset-feeding method, because they can easily be matched to a 50 Ω characteristic impedance without using any matching networks [49]–[52]. The whole structure is considered to be constructed on a Rogers RT5880 substrate [53], which has a thickness $h = 1.575$ mm and an electric permittivity $\epsilon_r = 2.2$. For the sake of consistency, the MPAA geometry is optimized by employing an effective PSO variant called "PSO with velocity mutation" [54]. The geometry parameters under optimization are: (i) the length L of the microstrip patches, (ii) the width W of the microstrip patches, (iii) the length t of the input transmission line, (iv) the inset depth t_d, and (v) the inset width t_w. The transmission line width is set equal to 5 mm, which results in a characteristic impedance of 50 Ω at 800 MHz. The goals of the optimization process are the highest possible forward gain and standing wave ratio values at the inputs of all the array elements below 1.2 (i.e., S-parameters $S_{m,m} \leq -20.8$ dB). The array elements are considered to be parallel to the yz-plane (see Fig. 3), with spacings $d_z = d_y = \lambda/2$, where λ is the free space wavelength at 800 MHz. Their input transmission lines are parallel to the y-axis, while the excitation sources are placed at the endpoints of these lines (the endpoints are represented by the "feed point" of Fig. 3). During the optimization process, all the feeding weights are considered to be equal to unity. The final dimensions of the optimized MPAA are $L = 124.6$ mm, $W = 152.4$ mm, $t = 5$ mm, $t_d = 39$ mm, and $t_w = 3.3$ mm. The gain of the optimized MPAA, when uniformly excited, is derived equal to 21 dBi.

In order to extract the values of $e_{\phi m}(\theta, \phi)$, $m = 1, 2, \ldots, M (M = 64)$, the MPAA is simulated 64 times. Each time, only one element is considered to be driven with a unitary weight (active element), while all the other elements are considered to be non-driven. The values of $e_{\phi m}(\theta, \phi)$, $m = 1, 2, \ldots, M$, are recorded with a stepsize of 0.1° for both θ and ϕ. As mentioned in section III, the feeding ports position ensures that E_θ is significantly lower compared to E_ϕ ($E_\theta << E_\phi$) inside a certain spherical sector, which means that the total radiation pattern of the antenna array can be well-approximated in this sector only by E_ϕ. This was validated with CST inside a spherical sector defined by $\theta \in [30^\circ, 150^\circ]$ and $\phi \in [-60^\circ, 60^\circ]$, and the outcome of this validation is presented in the next section. Our simulations are applied to an internal part of the above sector (i.e., a sector confined by $\theta \in [90^\circ, 150^\circ]$ and $\phi \in [-45^\circ, 45^\circ]$ as shown in Fig. 2), and therefore both the condition $E_\theta << E_\phi$ and the approximation of the total radiation pattern by E_ϕ apply to this internal sector as well. The reason for selecting this sector for our simulations has already been explained in section I. The storage required to save the electric field data for this spherical sector was measured approximately equal to 520 MB, which is a relatively small storage requirement according to the current technology standards, and thus it would not noticeably affect the cost of the beamformer in real-world use cases. Finally, due to the symmetry of the MPAA with respect to the xy-plane, the simulations needed to extract the values of $e_{\phi m}(\theta, \phi)$ can be reduced to half (i.e., 32 simulations).

VII. Validation of the Proposed Approach

To validate our proposed approach, we have implemented numerous tests, where we compare radiation patterns produced by the linear combination (6) of the phi-components $e_{\phi m}(\theta, \phi)$ ($m = 1, 2, \ldots, M$) of LEEPs using feeding weights derived from the modified ABF methods, versus radiation patterns of the total electric phi-component E_ϕ produced by a full-wave analysis of the MPAA in CST when applying the same feeding weights. The comparisons exhibit absolute resemblance. An example of these comparisons is shown in Fig. 4, where the radiation pattern extracted by the linear combination of $e_{\phi m}(\theta, \phi)$ ($m = 1, 2, \ldots, M$) using weights derived from the modified NSB method is compared with the radiation pattern of E_ϕ produced from CST simulation of the MPAA using the same feeding weights. In this example, a DIS with DOA $(\theta_1, \phi_1) = (130^\circ, 30^\circ)$ and a UIS with DOA $(\theta_2, \phi_2) = (120^\circ, 20^\circ)$ are considered to be received by the MPAA. The illustration of E_ϕ, when using weights derived

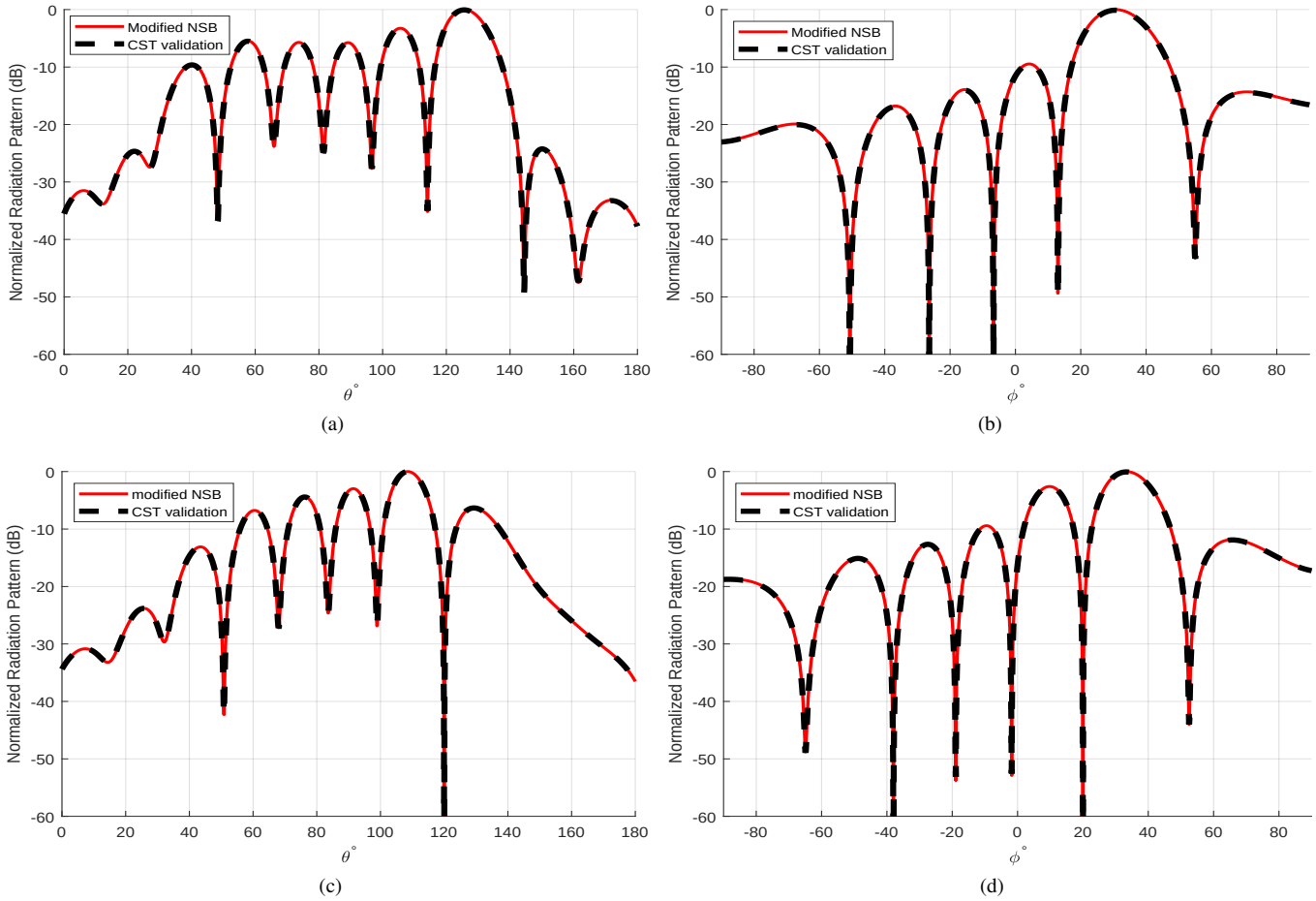

Fig. 4. Normalized radiation patterns of E_ϕ. In each graph two radiation patterns are depicted; One produced by the linear combination of LEEPs using weights derived by the modified NSB method, and the other by analyzing the whole array with CST using the same weights. One DIS at DOA $(\theta_1, \phi_1) = (130°, 30°)$ and one UIS at DOA $(\theta_2, \phi_2) = (120°, 20°)$ are received by the MPAA. In (a) and (b), the main lobe is depicted for constant values of $\phi = 30°$ and $\theta = 130°$, respectively. In (c) and (d), the null is depicted for constant values of $\phi = 20°$ and $\theta = 120°$, respectively.

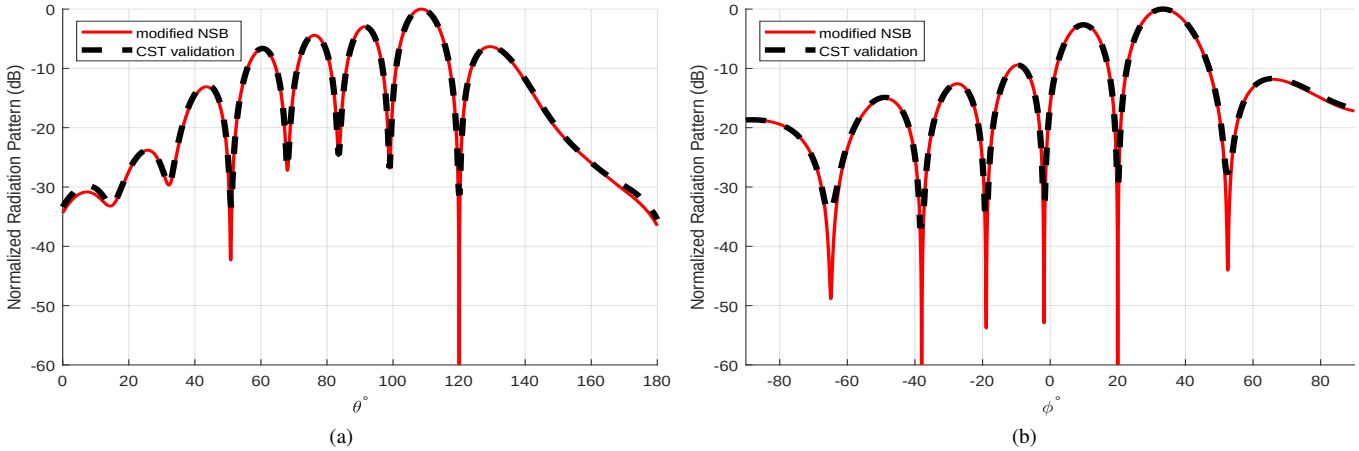

Fig. 5. Normalized radiation patterns. In each graph two radiation patterns are depicted; One illustrates E_ϕ, which is produced by the linear combination of LEEPs using weights derived by the modified NSB method, and the other illustrates the total electric field (i.e., considers both E_θ and E_ϕ) obtained through CST full-wave analysis. One DIS at DOA $(\theta_1, \phi_1) = (130°, 30°)$ and one UISs at DOA $(\theta_2, \phi_2) = (120°, 20°)$ are received by the MPAA. In (a), the null is depicted for constant $\phi = 20°$, while in (b), the null is depicted for constant $\theta = 120°$.

from the modified MVDR method, has been deemed by the authors as unnecessary because the weights derived from both modified methods are very close in magnitude and phase and therefore the respective radiation patterns are nearly identical.

Furthermore, we have verified that the theta-component E_θ of the total electric field is negligible compared with E_ϕ

($E_\theta << E_\phi$), as claimed in the first paragraph of section III and the last paragraph of section VI. To do so, we compare E_ϕ extracted by the linear combination of $e_{\phi m}(\theta, \phi)$ ($m = 1, 2, \ldots, M$) using weights derived from the modified ABF methods, with the total electric field (which takes into account both E_θ and E_ϕ) extracted through full-wave analysis of the MPAA in CST when applying the same feeding weights. The comparisons exhibit excellent resemblance inside the spherical sector defined by $\theta \in [30°, 150°]$ and $\phi \in [-60°, 60°]$. An example of these comparisons is illustrated in Fig. 5, where a DIS with DOA $(\theta_1, \phi_1) = (130°, 30°)$ and a UIS with DOA $(\theta_2, \phi_2) = (120°, 20°)$ are considered to be received by the MPAA, while the weights are derived from the modified NSB method. The difference in the null depth displayed in the graphs of this figure is due to the fact that, despite the condition $E_\theta << E_\phi$, the electric component E_ϕ decreases so much at null positions that it becomes considerably lower than the typically negligible E_θ. Therefore, the nulls of the total field cannot be as deep as the nulls of E_ϕ. However, this cannot be considered as a critical degradation of the null depth, because the nulls of the total electric field are still deep and they really do not affect the SINR value.

VIII. Performance and Temporal Response of the Proposed Approach

In order to examine the performance and temporal response of the proposed approach, we have performed two extensive statistical analyses. Both analyses are conducted for both modified NSB and MVDR methods and for two different SNR values, that is 0 dB and 10 dB. In the first statistical analysis, we evaluate how the performance of the modified ABF algorithms is affected by the angular distance between DOAs of the incoming signals. This analysis is performed for a fixed number of three incoming signals ($N = 3$), i.e., one DIS and two UISs. The angular distances $\Delta\theta$ and $\Delta\phi$ between any two adjacent DOAs of incoming signals are considered to be equal to 8°, 10° or 12° (three different scenarios). In the second statistical analysis, we evaluate the performance of the modified ABF methods in terms of the number of UISs, so we consider constant values of $\Delta\theta$ and $\Delta\phi$, specifically $\Delta\theta = \Delta\phi = 8°$. The performance is evaluated starting with one UIS and up to six UISs (six different scenarios). In every scenario, a large set of different DOA combinations is defined according to the following scheme:

1) Starting from the lower boundaries of both angular sectors ($\theta = 90°, \phi = -45°$), we define a set of N DOAs: $\{(90°, -45°), (90° + \Delta\theta, -45° + \Delta\phi), \ldots, (90° + (N-1)\Delta\theta, -45° + (N-1)\Delta\phi)\}$, where $\Delta\theta$, $\Delta\phi$ and N are defined according to the scenario under study.
2) We define N combinations of DOAs considering each time that DOA of DIS (θ_1, ϕ_1) is represented by a different pair of angles of the above set and all the other pairs are DOAs of UISs, i.e., $(\theta_1, \phi_1) = (90°, -45°)$ in the 1st combination, $(\theta_1, \phi_1) = (90° + \Delta\theta, -45° + \Delta\phi)$ in the 2nd, and finally $(\theta_1, \phi_1) = (90° + (N-1)\Delta\theta, -45° + (N-1)\Delta\phi)$ in the Nth.
3) We increase all the values of angle θ of the above set by 5° and we create a new set of N DOAs, i.e., $\{(95°, -45°), (95° + \Delta\theta, -45° + \Delta\phi), \ldots, (95° + (N-1)\Delta\theta, -45° + (N-1)\Delta\phi)\}$.
4) We additionally define N combinations of DOAs considering each time that DOA of DIS (θ_1, ϕ_1) is represented by a different pair of angles of the above set and the other pairs are DOAs of UISs (similarly to step 2).
5) We repeat steps 3 and 4 until any value of angle θ of the set exceeds 150° (upper boundary of the θ-sector).
6) We start again from the lower boundary of angle θ ($\theta = 90°$), but increase the value of angle ϕ by 5°, thus creating a new set of N DOAs, i.e., $\{(90°, -40°), (90° + \Delta\theta, -40° + \Delta\phi), \ldots, (90° + (N-1)\Delta\theta, -40° + (N-1)\Delta\phi)\}$.
7) We repeat steps 2-6 until any value of angle ϕ of the set exceeds 45° (upper boundary of the ϕ-sector).

In fact, the above-defined scheme generates all the possible DOA combinations, inside any spherical sector, with a stepsize of 5° for both angles θ and ϕ. The computer used for all the simulations performed in this paper is equipped with an Intel i7 5960X (eightcore) CPU and a 64 GB DDR4 RAM.

For each one of the above-described scenarios, we define a set of DOA combinations according to the previously-described scheme. Each DOA combination consists of N pairs of angles, i.e., one pair (θ_1, ϕ_1) that represents DOA of DIS and $N-1$ pairs $(\theta_2, \phi_2) \ldots (\theta_N, \phi_N)$ that represent DOAs of UISs. For each DOA combination, we calculate the divergence of the actual main lobe direction from (θ_1, ϕ_1), the divergences of the nulls directions from the respective DOAs $(\theta_2, \phi_2) \ldots (\theta_N, \phi_N)$ of UISs, and the SINR value. After all DOA combinations of the scenario are processed, we calculate the mean value and the standard deviation (std) of the main lobe divergence, the mean value and the standard deviation of the nulls divergences, the mean value and the standard deviation of the SINR, and the mean computational time per DOA combination. The divergences of the main lobe and the nulls are expressed by two separate angular divergences, one for θ and one for ϕ.

The results of the first statistical analysis are shown in Tables I and II for SNR = 0 dB and SNR = 10 dB, respectively. They reveal that, in all scenarios, both modified ABF methods are able to place nulls with exceptional accuracy, and therefore the SINR values are high. This is helped by the fact that a radiation pattern always has strong changes around a null, so the direction of a null can be determined by the ABF methods with great precision. On the other hand, the change in a radiation pattern around the peak of the main lobe is not as strong as in the case of a null. This does not help the ABF methods to determine the direction of the peak of the main lobe as accurately as in the case of a null, and this is verified by a small deviation of the main lobe from its expected direction (DOA of DIS).

The angular distance of DOAs of the incoming signals seems to have a noticeable effect only on the main lobe divergence, which improves (decreases) as this angular distance increases. An explanation for this is as follows: In fact, the angular distance of DOAs of two adjacent incoming signals is the expected distance between two adjacent nulls or between the main lobe and its nearest null. According to the number

TABLE I
1ST STATISTICAL ANALYSIS OF THE MODIFIED BEAMFORMING METHODS: SNR $= 0$ dB, $\Delta\theta = \Delta\phi = 8^\circ, 10^\circ, 12^\circ$ AND $N = 3$ (1 DIS & 2 UISS)

$\Delta\theta = \Delta\phi$	Method	Main lobe θ-divergence (deg) [mean/std]	Main lobe ϕ-divergence (deg) [mean/std]	Nulls θ-divergence (deg) [mean/std]	Nulls ϕ-divergence (deg) [mean/std]	SINR (dB) [mean/std]	Mean Time (μs)
8°	NSB	1.78/1.38	1.79/1.41	0.00/0.00	0.00/0.00	31.58/3.20	15
	MVDR	1.78/1.38	1.79/1.41	0.00/0.00	0.00/0.00	31.58/3.20	109
10°	NSB	0.97/1.02	1.66/1.37	0.00/0.00	0.00/0.00	31.79/3.24	15
	MVDR	0.97/1.02	1.66/1.37	0.00/0.02	0.00/0.03	31.79/3.24	108
12°	NSB	0.57/0.52	1.61/1.21	0.00/0.00	0.00/0.00	32.27/2.91	15
	MVDR	0.57/0.52	1.61/1.21	0.01/0.10	0.00/0.03	32.27/2.91	110

TABLE II
1ST STATISTICAL ANALYSIS OF THE MODIFIED BEAMFORMING METHODS: SNR $= 10$ dB, $\Delta\theta = \Delta\phi = 8^\circ, 10^\circ, 12^\circ$ AND $N = 3$ (1 DIS & 2 UISS)

$\Delta\theta = \Delta\phi$	Method	Main lobe θ-divergence (deg) [mean/std]	Main lobe ϕ-divergence (deg) [mean/std]	Nulls θ-divergence (deg) [mean/std]	Nulls ϕ-divergence (deg) [mean/std]	SINR (dB) [mean/std]	Mean Time (μs)
8°	NSB	1.78/1.38	1.79/1.41	0.00/0.00	0.00/0.00	41.58/3.20	15
	MVDR	1.78/1.38	1.79/1.41	0.00/0.00	0.00/0.00	41.58/3.20	108
10°	NSB	0.97/1.02	1.66/1.37	0.00/0.00	0.00/0.00	41.79/3.24	15
	MVDR	0.97/1.02	1.66/1.37	0.00/0.02	0.00/0.03	41.79/3.24	108
12°	NSB	0.57/0.52	1.61/1.21	0.00/0.00	0.00/0.00	42.27/2.91	15
	MVDR	0.57/0.52	1.61/1.21	0.01/0.10	0.00/0.03	42.27/2.91	110

TABLE III
2ND STATISTICAL ANALYSIS OF THE MODIFIED BEAMFORMING METHODS: SNR $= 0$ dB, $\Delta\theta = \Delta\phi = 8^\circ$ FOR 1 DIS & VARIOUS NUMBERS OF UISS

N	Method	Main lobe θ-divergence (deg) [mean/std]	Main lobe ϕ-divergence (deg) [mean/std]	Nulls θ-divergence (deg) [mean/std]	Nulls ϕ-divergence (deg) [mean/std]	SINR (dB) [mean/std]	Mean Time (μs)
2 (1 UIS)	NSB	2.07/1.18	1.91/1.57	0.00/0.00	0.00/0.00	31.11/3.54	10
	MVDR	2.07/1.18	1.91/1.57	0.00/0.00	0.00/0.00	31.11/3.54	105
3 (2 UISs)	NSB	1.78/1.38	1.79/1.41	0.00/0.00	0.00/0.00	31.58/3.20	15
	MVDR	1.78/1.38	1.79/1.41	0.00/0.00	0.00/0.00	31.58/3.20	109
4 (3 UISs)	NSB	1.87/1.46	2.06/1.43	0.00/0.00	0.00/0.00	30.63/3.79	16
	MVDR	1.87/1.46	2.06/1.43	0.02/0.07	0.01/0.05	30.64/3.78	136
5 (4 UISs)	NSB	1.82/1.48	1.95/1.31	0.00/0.00	0.00/0.00	30.77/3.64	20
	MVDR	1.82/1.48	1.95/1.31	0.01/0.04	0.01/0.05	30.78/3.63	147
6 (5 UISs)	NSB	2.01/1.56	2.23/1.28	0.00/0.00	0.00/0.00	29.61/4.45	21
	MVDR	2.00/1.56	2.22/1.28	0.04/0.08	0.03/0.07	29.63/4.42	149
7 (6 UISs)	NSB	1.96/1.56	2.17/1.22	0.00/0.00	0.00/0.00	29.53/4.54	25
	MVDR	1.96/1.56	2.17/1.22	0.00/0.02	0.00/0.02	29.53/4.54	152

of the array elements along each axis (y-axis or z-axis in our paper, see Fig. 3), this distance has a respective lower limit along each axis. So, when the distance becomes less than any of the above lower limits, the beamformer will face difficulty in placing the main lobe toward the expected direction (DOA of DIS), which results in a divergence of the main lobe from this direction. This also applies to nulls, but to a much lesser extent, because, as explained above, the strong changes of the radiation pattern around nulls help to place nulls toward the expected directions (DOAs of UISs) with much greater accuracy. However, if the number of the array elements along each axis increases, then the divergence of the main lobe will be kept at low values, even in cases when the angular distance of DOAs of the incoming signals is reduced (e.g., when $\Delta\theta = \Delta\phi = 8^\circ$). In this paper, only eight array elements per axis ($D = 8$) are used for practical reasons, because the use of a greater number of elements would only make the statistical analysis more time-consuming and yet would result in similar conclusions.

The SINR values exhibit only a slight improvement when $\Delta\theta$ and $\Delta\phi$ are increased (i.e., improvement of 0.7 dB when increasing angular distances from 8° to 12°). This is an expected behavior, because the accurate placement of nulls plays a major role in the SINR value, provided of course that the divergence of the main lobe is not excessive.

The results of the second statistical analysis are shown in Tables III and IV for SNR $= 0$ dB and SNR $= 10$ dB, respectively. The modified ABF methods exhibit a remarkable performance, even when increasing the number of UISs, only a slight change of the main lobe divergence is observed.

TABLE IV
2ND STATISTICAL ANALYSIS OF THE MODIFIED BEAMFORMING METHODS: SNR = 10 dB, $\Delta\theta = \Delta\phi = 8^\circ$ FOR 1 DIS & VARIOUS NUMBERS OF UISS

N	Method	Main lobe θ-divergence (deg) [mean/std]	Main lobe ϕ-divergence (deg) [mean/std]	Nulls θ-divergence (deg) [mean/std]	Nulls ϕ-divergence (deg) [mean/std]	SINR (dB) [mean/std]	Mean Time (μs)
2 (1 UIS)	NSB	2.07/1.18	1.91/1.57	0.00/0.00	0.00/0.00	41.11/3.54	10
	MVDR	2.07/1.18	1.91/1.57	0.00/0.00	0.00/0.00	41.11/3.54	105
3 (2 UISs)	NSB	1.78/1.38	1.79/1.41	0.00/0.00	0.00/0.00	41.58/3.20	15
	MVDR	1.78/1.38	1.79/1.41	0.00/0.00	0.00/0.00	41.58/3.20	108
4 (3 UISs)	NSB	1.87/1.46	2.06/1.43	0.00/0.00	0.00/0.00	40.63/3.79	16
	MVDR	1.87/1.46	2.06/1.43	0.02/0.07	0.01/0.05	40.64/3.78	134
5 (4 UISs)	NSB	1.82/1.48	1.95/1.31	0.00/0.00	0.00/0.00	40.77/3.64	20
	MVDR	1.82/1.48	1.95/1.31	0.01/0.04	0.01/0.05	40.78/3.63	147
6 (5 UISs)	NSB	2.01/1.56	2.23/1.29	0.00/0.00	0.00/0.00	39.61/4.45	21
	MVDR	2.01/1.56	2.23/1.28	0.00/0.01	0.00/0.01	39.61/4.44	148
7 (6 UISs)	NSB	1.96/1.56	2.17/1.22	0.00/0.00	0.00/0.00	39.53/4.54	25
	MVDR	1.96/1.56	2.17/1.22	0.00/0.02	0.00/0.02	39.53/4.54	154

TABLE V
1ST STATISTICAL ANALYSIS OF THE CONVENTIONAL BEAMFORMING METHODS: SNR = 0 dB, $\Delta\theta = \Delta\phi = 8^\circ, 10^\circ, 12^\circ$ AND $N = 3$ (1 DIS & 2 UISS)

$\Delta\theta = \Delta\phi$	Method	Main lobe θ-divergence (deg) [mean/std]	Main lobe ϕ-divergence (deg) [mean/std]	Nulls θ-divergence (deg) [mean/std]	Nulls ϕ-divergence (deg) [mean/std]	SINR (dB) [mean/std]	Mean Time (μs)
8°	NSB	53.57/27.09	2.26/2.95	3.96/1.22	3.42/1.22	1.28/9.11	14
	MVDR	53.66/27.20	2.17/2.68	3.96/1.22	3.42/1.22	1.33/9.04	110
10°	NSB	57.39/28.45	1.67/2.55	4.15/1.10	3.52/1.28	2.36/9.55	16
	MVDR	57.40/28.46	1.64/2.50	4.15/1.11	3.52/1.28	2.38/9.59	109
12°	NSB	56.85/28.44	1.16/1.85	3.90/0.99	3.44/1.07	4.65/10.28	16
	MVDR	56.85/28.44	1.16/1.85	3.89/1.00	3.43/1.07	4.67/10.27	109

Once again, the radiation pattern nulls are placed with high precision, with near-zero divergence, even when the number of UISs is increased (from 1 UIS to 6 UISs).

In both statistical analyses, the SNR value does not seem to affect the performance of the beamformers at all. Both statistical analyses reveal that the performance of the modified beamformers is excellent throughout all scenarios of escalating difficulty.

In terms of computational time, both statistical analyses show that the modified NSB method runs a lot faster compared to the modified MVDR method. This is expected because, as shown in (27), the modified NSB method calculates the inverse of $\mathbf{E}_\phi^{\mathrm{H}}\mathbf{E}_\phi$, which is an $N \times N$ matrix. On the other hand, as shown in (29), the modified MVDR method calculates the inverse of $\mathbf{R}_{xx}$, which is an $M \times M$ matrix. Since the antenna array consists of 64 elements, the modified MVDR method has to invert a 64×64 matrix, which is significantly larger compared to an $N \times N$ matrix, where $N = 2, 3, \ldots, 7$.

Finally, four 3D radiation patterns are given in Fig. 6 as examples, in order to visualize the precise radiation shaping achieved by the modified ABF methods. In all the examples, the scenario with the highest difficulty is visualized (1 DIS and 6 UISs). In Figs. 6a and 6b, the 3D radiation patterns of the MPAA are illustrated, respectively for $\mathrm{SNR} = 0$ dB and $\mathrm{SNR} = 10$ dB, when the array elements are driven with feeding weights derived from the modified NSB method. Similarly, in Figs. 6c and 6d, the 3D radiation patterns of the MPAA are depicted, respectively for $\mathrm{SNR} = 0$ dB and $\mathrm{SNR} = 10$ dB, when the array elements are driven with feeding weights derived from the modified MVDR method.

IX. COMPARISON WITH THE CONVENTIONAL NSB AND MVDR METHODS AND A PSO-BASED BEAMFORMER

In order to demonstrate the improvement achieved by the modified NSB and MVDR methods over their conventional counterparts, we repeat the 1st statistical analysis for $\mathrm{SNR} = 0$ dB using the conventional NSB and MVDR methods. In fact, instead of using the electric phi-vector expression given in (8), we use the theoretical steering vector expression given in (3), and therefore we treat the MPAA as a planar array composed of isotropic sources. The excitation weights extracted by the conventional methods are used to produce the radiation pattern of the MPAA through full-analysis in the CST environment. The results of the statistical analysis are presented in Table V. It seems that the conventional methods are incapable of steering the main lobe towards DOA of DIS, while introducing considerable divergences on the nulls directions. Consequently, the SINR value is really low. Moreover, not only do the modified methods perform significantly better, but they also require the same computational time compared to their conventional counterparts (see Table I in comparison with Table V). Therefore, the modified methods demonstrate a significant

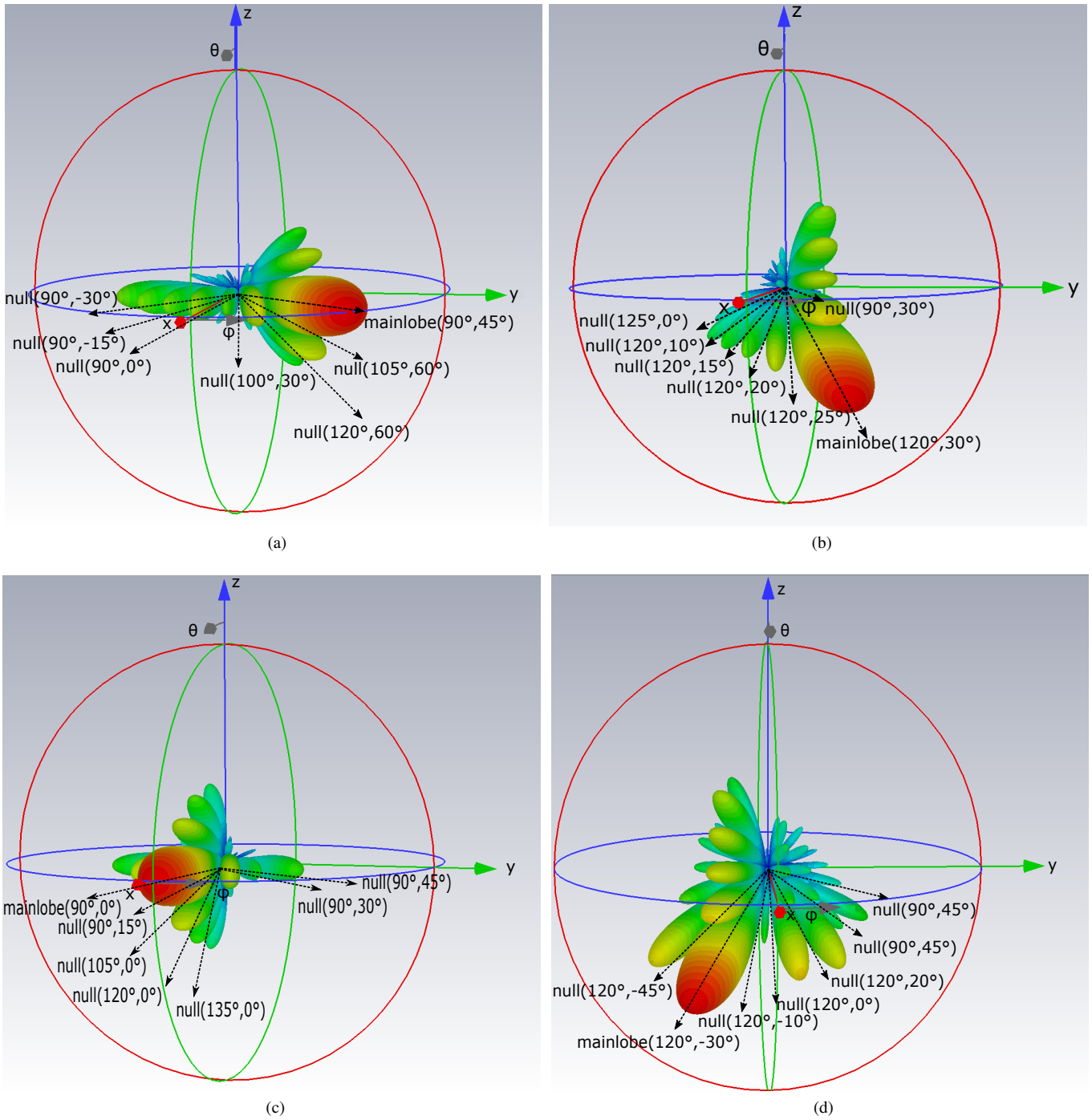

Fig. 6. 3D radiation patterns of the 64-element MPAA, simulated in CST, when the main lobe is steered towards DOA of DIS and six nulls are placed towards respective DOAs of UISs. In (a) and (b), the radiation patterns are derived using feeding weights calculated by the modified NSB method for SNR $= 0$ dB and SNR $= 10$ dB, respectively. In (c) and (d), the radiation patterns are derived using feeding weights calculated by the modified MVDR method for SNR $= 0$ dB and SNR $= 10$ dB, respectively.

improvement in terms of accuracy, while maintaining the same temporal response.

Furthermore, we compare the modified NSB and MVDR methods with a PSO-based beamforming algorithm, which has been chosen as an example of beamforming methods based on evolutionary optimization techniques. We select the first scenario of the first statistical analysis, i.e., SNR $= 0$ dB, $\Delta\theta = \Delta\phi = 8°$, $N = 3$ (1 DIS & 2 UISs), and we perform 100 trials. To help the PSO technique find the optimal solution as quickly as possible, the fitness function must be expressed through a single parameter that includes all the beamforming requirements. This parameter is chosen to be the SINR, because its maximization implies that the main lobe is steered toward DOA of DIS, while, at the same time, radiation pattern nulls are placed toward DOAs of respective UISs. Given that the PSO technique employed here is based

on the minimization of the fitness function, the fitness function will be defined as:

$$F = -\text{SINR} \tag{30}$$

where the SINR is expressed in dB. By minimizing F, the PSO technique reaches the maximum value of the SINR. The PSO-based beamformer requires 170 ms per DOA combination (5000 fitness evaluations) on average to achieve the desired beamforming requirements. However, the modified NSB and MVDR methods achieve similar results within microseconds (see Table I). Consequently, due to the significant difference in computational time, deterministic beamformers, like the modified NSB and MVDR methods, are more preferable for real-time processes compared to beamformers based on evolutionary optimization techniques.

Finally, it should be noted that, in order to have a fair comparison, the computer used in the statistical analysis of the conventional NSB and MVDR methods as well as in all the trials of the PSO-based beamformer is the same as the one used in all the statistical analyses of the modified NSB and MVDR methods (Intel i7 5960X (eightcore) CPU and a 64 GB DDR4 RAM).

X. Conclusion

By applying our proposed approach, both the particular non-isotropic radiation pattern of the array elements and the mutual coupling between them can effectively be incorporated as information into the steering vectors to accurately control the reception of incoming signals by a realistic planar antenna array. The validity of the proposed approach was confirmed through numerous comparisons between radiation patterns produced by applying the proposed approach and radiation patterns extracted by full-wave analysis of the planar antenna array using CST.

By employing our approach, the NSB and MVDR methods can properly be modified to perform beamforming in 3D space. As shown by the two statistical analyses carried out in this paper, the modified beamformers exhibit remarkable performance with near-zero divergences of nulls from DOAs of UISs, minor divergence of the main lobe from DOA of DIS, and high SINR values. Furthermore, the modified beamformers are robust, since there is almost no degradation in their performance, even when increasing the number of the incoming signals. It was also shown that the modified beamformers outperform their conventional counterparts regarding the accuracy of the main lobe direction and the accuracy of nulls placement, while maintaining the same temporal response. In addition, the utilization of the modified ABF methods is not limited to the realistic planar antenna array used as an example in this paper, but can also be extended to any type or geometry of antenna array, as long as LEEPs of the array in use are available. Finally, the modified ABF methods work really fast, their temporal response is much higher than that of evolutionary optimization based beamformers, and they require little memory space. All these advantages make the new approach suitable for real-world applications.

References

[1] L. C. Godara, *Smart antennas*. CRC press, 2004.

[2] F. Gross, *Smart antennas for wireless communications*. McGraw-Hill Professional, 2005.

[3] J. Li and P. Stoica, *Robust adaptive beamforming*. Wiley Online Library, 2006.

[4] C. A. Olen and R. Compton, "A numerical pattern synthesis algorithm for arrays," *IEEE Trans. Antennas Propag.*, vol. 38, no. 10, pp. 1666–1676, 1990.

[5] P. Kasemir, N. Sutton, M. Radway, B. Jeong, T. Brown, and D. S. Filipovič, "Wideband analog and digital beamforming," in *2009 9th International Conference on Telecommunication in Modern Satellite, Cable, and Broadcasting Services*, 2009, pp. 372–375.

[6] L. Zhang, W. Liu, and R. J. Langley, "Adaptive beamforming with real-valued coefficients based on uniform linear arrays," *IEEE Trans. Antennas Propag.*, vol. 59, no. 3, pp. 1047–1053, 2010.

[7] J. A. Srar, K.-S. Chung, and A. Mansour, "Adaptive array beamforming using a combined LMS-LMS algorithm," *IEEE Trans. Antennas Propag.*, vol. 58, no. 11, pp. 3545–3557, 2010.

[8] S. Kim and B. Shim, "Aod-based statistical beamforming for cell-free massive mimo systems," in *2018 IEEE 88th Vehicular Technology Conference (VTC-Fall)*, 2018, pp. 1–5.

[9] S. H. Lim, S. Kim, B. Shim, and J. W. Choi, "Efficient beam training and sparse channel estimation for millimeter wave communications under mobility," *IEEE Trans. Commun.*, vol. 68, no. 10, pp. 6583–6596, 2020.

[10] G. Gottardi, L. Poli, P. Rocca, A. Montanari, A. Aprile, and A. Massa, "Optimal monopulse beamforming for side-looking airborne radars," *IEEE Antennas Wireless Propag. Lett.*, vol. 16, pp. 1221–1224, 2016.

[11] W. P. Keizer, "Fast low-sidelobe synthesis for large planar array antennas utilizing successive fast fourier transforms of the array factor," *IEEE Trans. Antennas Propag.*, vol. 55, no. 3, pp. 715–722, 2007.

[12] M. Roshanaei, C. Lucas, and A. Mehrabian, "Adaptive beamforming using a novel numerical optimisation algorithm," *IET microwaves, antennas & propagation*, vol. 3, no. 5, pp. 765–773, 2009.

[13] L. Poli, P. Rocca, G. Oliveri, and A. Massa, "Harmonic beamforming in time-modulated linear arrays," *IEEE Trans. Antennas Propag.*, vol. 59, no. 7, pp. 2538–2545, 2011.

[14] Z. D. Zaharis and T. V. Yioultsis, "A novel adaptive beamforming technique applied on linear antenna arrays using adaptive mutated boolean pso," *Prog. Electromagn. Res.*, vol. 117, pp. 165–179, 2011.

[15] G. Mahanti, V. B. Bikkani, and S. Mandal, "Placement of wide nulls in the radiation pattern of a linear array antenna using iterative fast fourier transform," in *2012 IEEE International Conference on Signal Processing, Communication and Computing (ICSPCC 2012)*, 2012, pp. 552–555.

[16] L. Yang, G. Ren, W. Zhai, and Z. Qiu, "Beamforming based receiver scheme for DVB-T2 system in high speed train environment," *IEEE Trans. Broadcast.*, vol. 59, no. 1, pp. 146–154, 2012.

[17] N. A. Sutton and D. S. Filipovic, "V-band monolithically integrated four-arm spiral antenna and beamforming network," in *Proceedings of the 2012 IEEE International Symposium on Antennas and Propagation*. IEEE, 2012, pp. 1–2.

[18] A. Young, M. V. Ivashina, R. Maaskant, O. A. Iupikov, and D. B. Davidson, "Improving the calibration efficiency of an array fed reflector antenna through constrained beamforming," *IEEE Trans. Antennas Propag.*, vol. 61, no. 7, pp. 3538–3545, 2013.

[19] D. Prinsloo, M. Ivashina, R. Maaskant, and P. Meyer, "Beamforming strategies for active multi-mode antennas: Maximum gain, signal-to-noise ratio, and polarization discrimination," in *2014 International Conference on Electromagnetics in Advanced Applications (ICEAA)*. IEEE, 2014, pp. 507–510.

[20] O. Iupikov, M. Ivashina, K. Pontoppidan, P. Nielsen, C. Cappellin, N. Skou, S. S. Søbjærg, A. Ihle, D. Hartmann, and K. v't Klooster, "An optimal beamforming algorithm for phased-array antennas used in multi-beam spaceborne radiometers," in *2015 9th European Conference on Antennas and Propagation (EuCAP)*. IEEE, 2015, pp. 1–5.

[21] O. A. Iupikov, M. V. Ivashina, C. Cappellin, and N. Skou, "Digital-beamforming array antenna technologies for future ocean-observing satellite missions," in *2016 IEEE International Symposium on Antennas and Propagation (APSURSI)*. IEEE, 2016, pp. 1377–1378.

[22] O. A. Iupikov, M. V. Ivashina, N. Skou, C. Cappellin, K. Pontoppidan, and C. G. van't Klooster, "Multibeam focal plane arrays with digital beamforming for high precision space-borne ocean remote sensing," *IEEE Trans. Antennas Propag.*, vol. 66, no. 2, pp. 737–748, 2017.

[23] M. S. Rabbani, J. Churm, and A. Feresidis, "Millimetre-wave beam steerable leaky-wave antenna for 5G systems," in *12th European Conference on Antennas and Propagation (EuCAP 2018)*, 2018, pp. 1–4.

[24] O. Manoochehri, D. Erricolo, A. Darvazehban, and F. Monticone, "Design of compact beam-steering active slot antennas with a metasurface reflector," in *2019 United States National Committee of URSI National Radio Science Meeting (USNC-URSI NRSM)*. IEEE, 2019, pp. 1–2.

[25] J. Wu and B. Shim, "Transmit power minimization in intelligent reflecting surfaces-aided uplink communications," in *2020 IEEE REGION 10 CONFERENCE (TENCON)*. IEEE, 2020, pp. 108–112.

[26] ——, "Power minimization of intelligent reflecting surface-aided uplink iot networks," in *2021 IEEE Wireless Communications and Networking Conference (WCNC)*. IEEE, 2021, pp. 1–6.

[27] N. Anselmi, P. Rocca, M. Salucci, and A. Massa, "Optimisation of excitation tolerances for robust beamforming in linear arrays," *IET Microwaves, Antennas & Propagation*, vol. 10, no. 2, pp. 208–214, 2016.

[28] A. E. Zooghby, C. Christodoulou, and M. Georgiopoulos, "Neural network-based adaptive beamforming for one-and two-dimensional antenna arrays," *IEEE Trans. Antennas Propag.*, vol. 46, no. 12, pp. 1891–1893, 1998.

[29] X. Song, J. Wang, and X. Niu, "Robust adaptive beamforming algorithm based on neural network," in *2008 IEEE International Conference on Automation and Logistics*. IEEE, 2008, pp. 1844–1849.

[30] Z. D. Zaharis, K. A. Gotsis, and J. N. Sahalos, "Adaptive beamforming with low side lobe level using neural networks trained by mutated boolean pso," *Prog. Electromagn. Res.*, vol. 127, pp. 139–154, 2012.

[31] Z. D. Zaharis, C. Skeberis, T. D. Xenos, P. I. Lazaridis, and J. Cosmas, "Design of a novel antenna array beamformer using neural networks trained by modified adaptive dispersion invasive weed optimization based data," *IEEE Trans. Broadcast.*, vol. 59, no. 3, pp. 455–460, 2013.

[32] H. Steyskal and J. S. Herd, "Mutual coupling compensation in small array antennas," *IEEE Trans. Antennas Propag.*, vol. 38, no. 12, pp. 1971–1975, 1990.

[33] Z. Zaharis, T. Samaras, E. Vafiadis, and J. Sahalos, "Antenna array design by the orthogonal method in conjunction with element patterns," *Microwave and optical technology letters*, vol. 48, no. 8, pp. 1578–1583, 2006.

[34] Z. Ye and C. Liu, "Non-sensitive adaptive beamforming against mutual coupling," *IET Signal Processing*, vol. 3, no. 1, pp. 1–6, 2009.

[35] B. Liao and S.-C. Chan, "Adaptive beamforming for uniform linear arrays with unknown mutual coupling," *IEEE Antennas Wireless Propag. Lett.*, vol. 11, pp. 464–467, 2012.

[36] X. Yang, J. Xie, H. Li, and Z. He, "Robust adaptive beamforming of coherent signals in the presence of the unknown mutual coupling," *IET Communications*, vol. 12, no. 1, pp. 75–81, 2017.

[37] Z. Zheng, K. Liu, W.-Q. Wang, Y. Yang, and J. Yang, "Robust adaptive beamforming against mutual coupling based on mutual coupling coefficients estimation," *IEEE Trans. Veh. Technol.*, vol. 66, no. 10, pp. 9124–9133, 2017.

[38] Y. Liu, X. Huang, K. Da Xu, Z. Song, S. Yang, and Q. H. Liu, "Pattern synthesis of unequally spaced linear arrays including mutual coupling using iterative FFT via virtual active element pattern expansion," *IEEE Trans. Antennas Propag.*, vol. 65, no. 8, pp. 3950–3958, 2017.

[39] B. Bahreini, H. Oraizi, N. Noori, and P. Mousavi, "Optimum design of a beam-forming array of S-shaped DRA elements with a superstrate on an SIW feed for 5G mobile systems," *IEEE Antennas Wireless Propag. Lett.*, 2019.

[40] S. Kim and S. Nam, "A compact and wideband linear array antenna with low mutual coupling," *IEEE Trans. Antennas Propag.*, vol. 67, no. 8, pp. 5695–5699, 2019.

[41] Z. D. Zaharis, I. P. Gravas, P. I. Lazaridis, T. V. Yioultsis, C. S. Antonopoulos, and T. D. Xenos, "An effective modification of conventional beamforming methods suitable for realistic linear antenna arrays," *IEEE Trans. Antennas Propag.*, vol. 68, no. 7, pp. 5269–5279, 2020.

[42] D. M. Pozar, "The active element pattern," *IEEE Trans. Antennas Propag.*, vol. 42, no. 8, pp. 1176–1178, 1994.

[43] B. Friedlander, "Antenna array manifolds for high-resolution direction finding," *IEEE Trans. Signal Process.*, vol. 66, no. 4, pp. 923–932, 2018.

[44] CST Studio Suite. [Online]. Available: https://www.3ds.com

[45] P. Demarcke, H. Rogier, R. Goossens, and P. De Jaeger, "Beamforming in the presence of mutual coupling based on constrained particle swarm optimization," *IEEE Trans. Antennas Propag.*, vol. 57, no. 6, pp. 1655–1666, 2009.

[46] L. A. Greda, A. Winterstein, D. L. Lemes, and M. V. T. Heckler, "Beamsteering and beamshaping using a linear antenna array based on particle swarm optimization," *IEEE Access*, vol. 7, pp. 141 562–141 573, 2019.

[47] J. Patin and S. K. Sharma, "Dual band single feed dielectric resonator antenna with linear and circular polariziations for Ku-band," in *2011 IEEE International Symposium on Antennas and Propagation (APSURSI)*. IEEE, 2011, pp. 1678–1681.

[48] P. K. Mishra, S. Yadav, K. Jaiswal, and R. Singh, "Dual band key-shaped microstrip patch antenna for c/x band applications," in *Proceedings of the International Conference on Advances in Electronics, Electrical & Computational Intelligence (ICAEEC)*, 2019.

[49] C. A. Balanis, *Antenna Theory: Analysis and Design*, 3rd ed. New York, NY, USA: Wiley-Interscience, 2005, pp. 816–826.

[50] Y. Hu, D. R. Jackson, J. T. Williams, S. A. Long, and V. R. Komanduri, "Characterization of the input impedance of the inset-fed rectangular microstrip antenna," *IEEE Trans. Antennas Propag.*, vol. 56, no. 10, pp. 3314–3318, 2008.

[51] M. Matin and A. Sayeed, "A design rule for inset-fed rectangular microstrip patch antenna," *WSEAS Transactions on Communications*, vol. 9, no. 1, pp. 63–72, 2010.

[52] C. Mbinack, B. Bodo, J.-S. A. Eyébé Fouda, and E. Tonye, "Inset-fed rectangular microstrip patch antenna bandwidth enhancement," *Microwave and Optical Technology Letters*, vol. 61, no. 2, pp. 562–567, 2019.

[53] Rogers Corporation. [Online]. Available: https://www.rogerscorp.com/

[54] Z. D. Zaharis, I. P. Gravas, P. I. Lazaridis, I. A. Glover, C. S. Antonopoulos, and T. D. Xenos, "Optimal LTE-protected LPDA design for DVB-T reception using particle swarm optimization with velocity mutation," *IEEE Trans. Antennas Propag.*, vol. 66, no. 8, pp. 3926–3935, Aug. 2018.

Zaharias D. Zaharis (M'13–SM'15) received the B.Sc. degree in physics, the M.Sc. degree in electronics, the Ph.D. degree in antennas and propagation modeling for mobile communications, and the Diploma degree in electrical and computer engineering from the Aristotle University of Thessaloniki, Thessaloniki, Greece, in 1987, 1994, 2000, and 2011, respectively. From 2002 to 2013, he was with the Administration of the Telecommunications Network, Aristotle University of Thessaloniki. Since 2013, he has been with the Department of Electrical and Computer Engineering, Aristotle University of Thessaloniki. He has been involved in several international research projects, such as EU Horizon 2020 MOTOR5G and RECOMBINE. His current research interests include design and optimization of antennas and microwave circuits, signal processing on smart antennas, development of evolutionary optimization algorithms, and neural networks. Dr. Zaharis is a member of the Technical Chamber of Greece. He is currently serving as an Associate Editor for IEEE ACCESS.

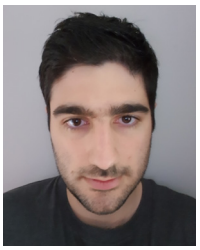

Ioannis P. Gravas (S'17) received the Diploma degree in electrical and computer engineering in 2017 and the Ph.D. degree in 2021 from the Aristotle University of Thessaloniki, Greece. His research interests include beamforming and direction of arrival estimation techniques, design and optimization of antennas, and evolutionary optimization algorithms.

Pavlos I. Lazaridis (M'13–SM'15) received the B.Sc. degree in electrical engineering from the Aristotle University of Thessaloniki, Thessaloniki, Greece, in 1990, the M.Sc. degree in electronics from Université Pierre and Marie Curie, Paris, France, in 1992, and the Ph.D. degree from École Nationale Supérieure des Télécommunications (ENST) Paris, Paris, in 1996. From 1991 to 1996, he was involved with research for France Télécom, Paris, France, and teaching at ENST Paris. In 1997, he became the Head of the Antennas and Propagation Laboratory, Télédiffusion de France/France Télécom Research Center (TDF-C2R Metz). From 1998 to 2002, he was a Senior Examiner at the European Patent Office (EPO), The Hague, The Netherlands. From 2002 to 2014 he was involved with teaching and research at the ATEI of Thessaloniki, Thessaloniki, Greece, and Brunel University, London, U.K. He is currently a Professor of electronic and electrical engineering at the University of Huddersfield, Huddersfield, U.K. He is a member of the Institution of Engineering and Technology (IET) and a fellow of the Higher Education Academy.

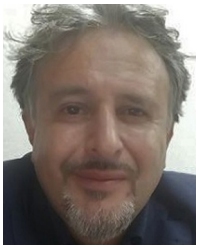

Traianos V. Yioultsis (M'09) received the Diploma and Ph.D. degrees in electrical and computer engineering from the Aristotle University of Thessaloniki, Thessaloniki, Greece, in 1992 and 1998, respectively. From 2001 to 2002, he was a Post-Doctoral Research Associate with the Department of Electrical and Computer Engineering, University of Illinois at Urbana–Champaign, Champaign, IL, USA. Since 2002, he has been with the Department of Electrical and Computer Engineering, Aristotle University of Thessaloniki, where he is currently a Professor. His current interests include the analysis and design of antennas and microwave circuits with fast computational techniques, and the modeling of complex wave propagation problems. Dr. Yioultsis has served as a member of the Editorial Board for IEEE COMMUNICATIONS LETTERS and several international conferences.

Thomas D. Xenos was born in Thessaloniki, Greece. He received the Diploma degree in electrical engineering from the University of Patras, Patras, Greece, in 1978, and the Ph.D. degree in wireless communications from the Aristotle University of Thessaloniki, Thessaloniki, Greece, in 1991. Since then, he has joined the Department of Electrical and Computer Engineering, Aristotle University of Thessaloniki, where he is currently a Professor. He has participated in many national and international projects. He has authored over 85 scientific articles. His research interests include wireless communications, radio-wave propagation, nonionizing electromagnetic radiation measurements, and electromagnetic compatibility.